

Comment on “A Supervoid Imprinting the Cold Spot in the Cosmic Microwave Background”

James P. Zibin^{1,*}

¹*Department of Physics & Astronomy
University of British Columbia, Vancouver, BC, V6T 1Z1 Canada
(Dated: August 20, 2014)*

Recently Finelli et al. [arXiv:1405.1555] found evidence for a relatively nearby ($z \simeq 0.16$) void in a galaxy catalogue in the direction of the cosmic microwave background (CMB) Cold Spot. Using a perturbative calculation, they also claimed that such a void would produce a CMB decrement comparable to that of the observed Cold Spot, mainly via the nonlinear Rees-Sciama effect. Here I calculate the effect of such a void using a fully general relativistic model and show that, to the contrary, the linear integrated Sachs-Wolfe effect dominates and produces a substantially weaker decrement than observed.

INTRODUCTION

Recently Finelli et al. [1] (hereafter FGKPS) examined the WISE-2MASS galaxy catalogue and found evidence for a void in the direction of the cosmic microwave background (CMB) Cold Spot. They furthermore calculated the anisotropy generated by such a void on the CMB and claimed that the void could explain most of the Cold Spot decrement, mainly due to the nonlinear Rees-Sciama (RS) effect. In this brief Comment, I calculate the effect on the CMB of the best-fit void found by FGKPS, using the fully nonlinear spherically symmetric Λ -Lemaître-Tolman-Bondi (ALTB) spacetime [2], sourced by dust and Λ , as developed for [3]. I consider a standard Λ CDM universe with *Planck* best-fit parameters [4].

I first point out a matter of nomenclature. Although FGKPS state “We model the underdensity...with a ALTb model”, they actually perform a perturbative RS calculation using the linearized density (or metric) perturbation. It is not enough for a structure to be spherically symmetric to be referred to as a ALTb model—the evolution must also be performed using fully nonlinear general relativity, which FGKPS do not do.

THE FGKPS PROFILE

The spherically symmetric spacetime is described by the metric

$$ds^2 = -dt^2 + \frac{Y'^2}{1-K} dr^2 + Y^2 d\Omega^2, \quad (1)$$

for comoving coordinate r and radial derivative $' = d/dr$. FGKPS adopt the curvature function profile

$$K(r) = K_0 r^2 \exp\left(-\frac{r^2}{r_0^2}\right). \quad (2)$$

It is possible to show that, in the linear regime, the curvature function is related to the comoving curvature metric

perturbation, $\psi_q(r)$, via

$$K(r) = 2r\psi_q'(r). \quad (3)$$

Therefore the FGKPS profile corresponds to

$$\psi_q(r) = -\frac{1}{4}K_0 r_0^2 \exp\left(-\frac{r^2}{r_0^2}\right). \quad (4)$$

The comoving perturbation ψ_q is time-independent in a dust or dust + Λ background, but is related to the time-dependent zero-shear (or longitudinal) gauge metric perturbation, ψ_σ , via

$$\psi_\sigma(t, r) = \frac{3}{5}g(t)\psi_q(r), \quad (5)$$

where $g(t)$ is the growth suppression factor accounting for the suppression due to Λ domination. The relativistic Poisson equation gives for the comoving gauge matter perturbation

$$\begin{aligned} \frac{\delta\rho_q(t, r)}{\rho_m} &= \frac{2}{5} \frac{g(t)}{\Omega_m} \frac{\nabla^2}{a^2 H^2} \psi_q(r) \\ &= \frac{3}{5} \frac{g(t)}{a^2 H^2 \Omega_m} K_0 \left[1 - \frac{2}{3} \frac{r^2}{r_0^2}\right] \exp\left(-\frac{r^2}{r_0^2}\right). \end{aligned} \quad (6)$$

This agrees with the form of the density contrast in FGKPS [their Eq. (2)], and allows us to identify their density contrast amplitude with

$$\delta_0 = -\frac{3}{5} \frac{g(t)}{a^2 H^2 \Omega_m} K_0. \quad (8)$$

FGKPS calculate the RS anisotropy for this profile, and write its central amplitude $A \equiv -\delta T(\theta = 0)$ as

$$A = 51.0 \mu\text{K} \left(\frac{r_0 h}{155.3 \text{ Mpc}}\right)^3 \left(\frac{\delta_0}{0.2}\right)^2. \quad (9)$$

(Note that here I quote the updated relation from [5], which appears to agree better with the values plotted in Fig. 3 of FGKPS than the relation for A given in FGKPS.) The cubic dependence of A on the radius and

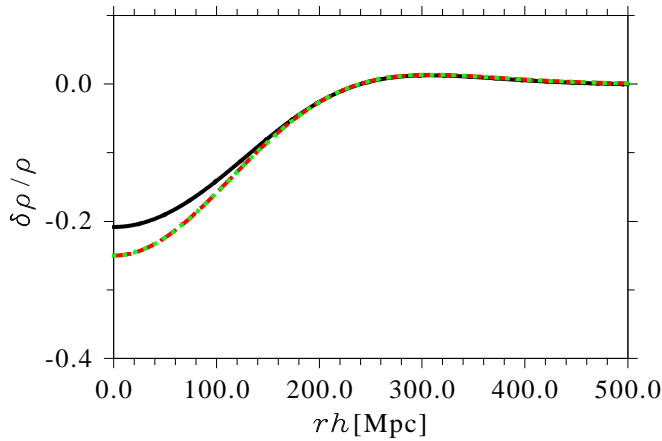


FIG. 1: Exact ALTB (solid, black curve), linearized ALTB (red, dashed), and FGKPS best-fit (green, dotted) three-dimensional density contrast. Here the ALTB model is chosen so the linearized ALTB contrast matches that of FGKPS.

quadratic dependence on density contrast are well-known features of the RS effect in an Einstein-de Sitter (EdS) background (see, e.g., [6, 7]).

Finally, FGKPS fit their density profile to the WISE-2MASS galaxy distribution, and the predicted anisotropy to CMB data, finding best-fit parameters

$$\delta_0 = 0.25 \pm 0.10, \quad (10)$$

$$r_0 h = (195 \pm 35) \text{ Mpc}, \quad (11)$$

$$z_0 = 0.155 \pm 0.037, \quad (12)$$

where z_0 is the redshift of the void centre. Eq. (9) then gives central amplitude $A = 158 \mu\text{K}$ for the best-fit profile, which appears to be consistent with the anisotropy profiles plotted in Fig. 3 of FGKPS (assuming subdominant integrated Sachs-Wolfe (ISW) effect and minor effects due to angular binning).

ALTB CALCULATION

In order to calculate with the ALTB spacetime, we must fix the curvature function amplitude K_0 in Eq. (2) [I will always fix the radius r_0 to the FGKPS best-fit value Eq. (11)]. There are two ways to do this. First, we can use Eqs. (8) and (10) to produce a ALTB profile with the same *linearized* density contrast as the FGKPS best fit. The result is plotted in Fig. 1. In this case the nonlinear contrast is smaller than that of the FGKPS best fit, as expected since nonlinear growth suppresses underdense contrast. The other approach is to choose K_0 so that the *exact* ALTB contrast matches the FGKPS best fit; this is plotted in Fig. 2. Note that the nonlinear growth changes the *shape* of the profile; I have chosen the *amplitudes* (central values) to match.

Although the difference between these two approaches is small, I choose the latter, i.e. I choose the exact ALTB

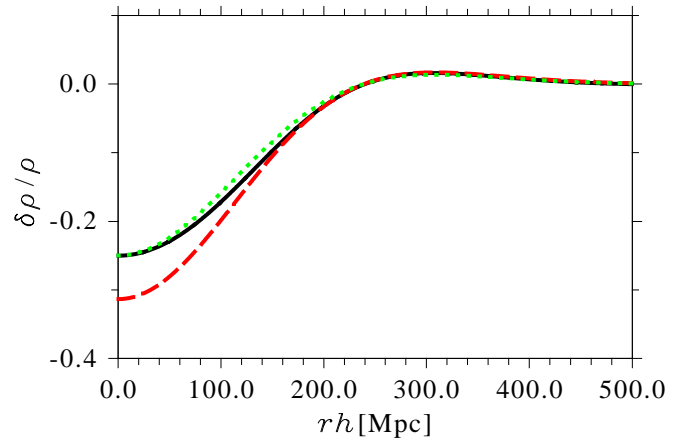


FIG. 2: As Fig. 1, but here the ALTB model is chosen so the exact ALTB contrast matches that of the FGKPS best fit.

contrast to match the FGKPS best fit. This is because this choice corresponds to a larger density contrast which will conservatively produce a larger CMB anisotropy (and in particular should produce a larger RS/ISW ratio). This corresponds to the value $K_0 r_0^2 = -0.00087$.

Finally I am ready to calculate the CMB anisotropies. The ALTB solution is calculated as in [3] by numerically evolving Einstein's equations using independent formulations as checks, including that described in [8]. I also monitor the constraints and compare with LTB (i.e. ALTB with $\Lambda = 0$) and linear theory in the appropriate regimes. The exact anisotropies are calculated by evolving null geodesics from the observer to the last scattering surface, as described in [9, 10].

The anisotropies due to the linearized ALTB solution [Eqs. (4) or (5)] can be calculated using

$$\frac{\delta T}{T} = 2 \int \dot{\psi}_\sigma dt + \left(\frac{5}{3g} - 1 \right) \frac{n_\mu \psi_\sigma^{;\mu}}{H}, \quad (13)$$

where n_μ is the line-of-sight spatial direction [11]. The first term above is the familiar ISW effect, and the second term is the local dipole due to the “bulk flow” associated with the void. Even though the curvature profile is exponentially damped at large r , we will see that at the FGKPS best-fit distance z_0 the local dipole actually dominates over the ISW.

Figure 3 shows the anisotropy calculated exactly via raytracing in the ALTB spacetime as well as the linearized approximation using Eq. (13). We can see that the local dipolar anisotropy does indeed dominate. But we can also see that the linearized approximation (which does not incorporate the RS effect) agrees well with the exact calculation (which must include it), which suggests that the ISW dominates over RS.

We can see this more clearly by subtracting the local dipole contribution from both exact and linearized anisotropies, as in Fig. 4. Here we see that the anisotropy calculated from the exact ALTB solution agrees very well

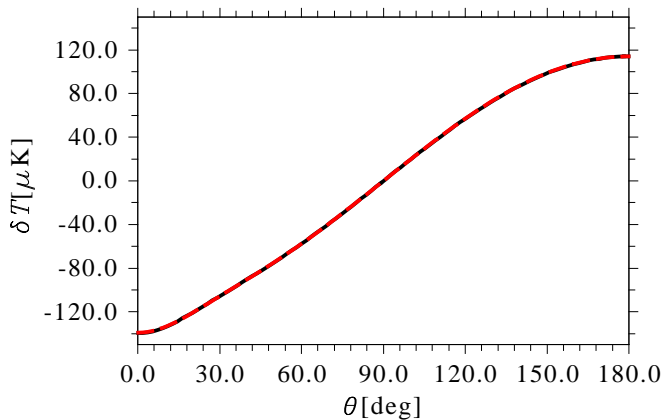


FIG. 3: Temperature anisotropy calculated exactly using the ALT solution (solid, black curve) and using the linearized relation, Eq. (13) (dashed, red). The two curves are almost indistinguishable and are dominated by the local dipole.

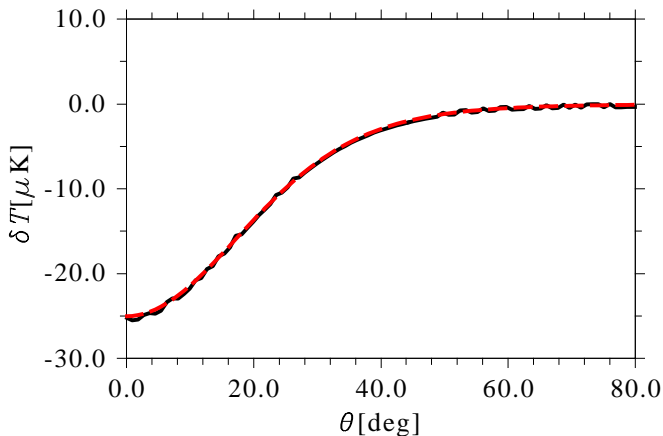


FIG. 4: As Fig. 3, but with the (linear) local dipole subtracted from both curves. The ISW clearly strongly dominates the total anisotropy.

with the linearized, ISW anisotropy. This demonstrates that the RS effect is subdominant for a void of this size, depth, and distance. The central anisotropy is approximately $-25 \mu\text{K}$, which agrees well with the estimate of $-20 \mu\text{K}$ from [12], based on the linear ISW effect.

Finally, in order to demonstrate that the ALT code can indeed capture the RS effect, I repeat the above calculations for a profile with the same width but 10 times the depth of the FGKPS profile, and centred at $z_0 = 1$. The greater depth and distance both ensure a larger RS/ISW ratio. Figure 5 shows that in this case the nonlinear effects are indeed important.

DISCUSSION

The question remains as to why the RS prediction of FGKPS, Eq. (9), is so much larger than the nonlinear ef-

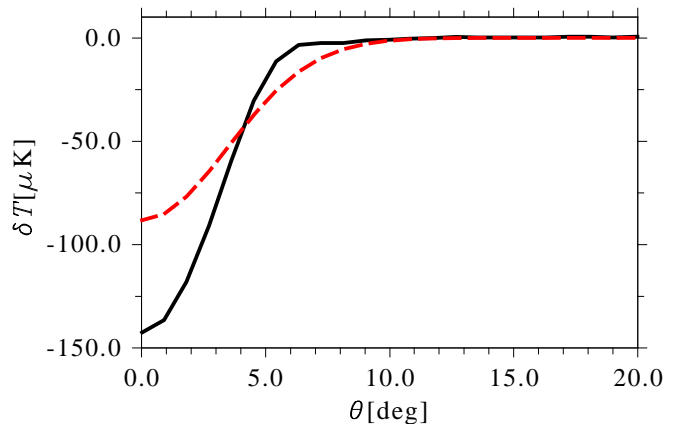


FIG. 5: As Fig. 4, but for a profile with 10 times the amplitude of the FGKPS profile and located at $z_0 = 1$. The nonlinear contribution (RS effect) is now clearly apparent.

fect seen in the full ALT calculation. Although the RS effect is well studied in an EdS (dust) background, leading, as already mentioned, to the dependences on radius and contrast seen in Eq. (9), the effect has been much less studied in a dust + Λ background. However, Ref. [13] studied the RS effect in this latter case, employing second order, thin shell, and fully nonlinear ALT methods. They found that the RS (nonlinear contribution to the anisotropies) is heavily suppressed in the realistic Λ CDM case with respect to the dust-dominated case, and that for comparable void size and depth to the FGKPS profile the linear (ISW) anisotropy dominates.

I have also repeated these calculations using different radial profiles $K(r)$, including strongly non-compensated profiles, by fitting the profile parameters to closely match the density profile of FGKPS. In all cases I find that the ISW effect dominates over the RS effect and is of comparable magnitude to that of the FGKPS profile. Of course, it is entirely possible that the void discussed in FGKPS contributes partly to the Cold Spot anisotropy. But it is clear that most of the anisotropy must be sourced elsewhere, since the Cold Spot amplitude is considerably larger than $-25 \mu\text{K}$: the Cold Spot has a deep “core” of roughly 5° radius and $\sim 150 \mu\text{K}$ depth, surrounded by a shallower cold region out to perhaps 10° radius (see, e.g., FGKPS or [14]). In addition, the angular size of the anisotropy shown in Fig. 4 (i.e. 30° – 40°) is much larger than that of the observed Cold Spot. Although some exotic source is always a possibility, a combination of the local void with a fluke fluctuation at last scattering might appear most economical. Indeed such a scenario was found to be most likely in [15].

Acknowledgments

This research was supported by the Canadian Space Agency.

* Electronic address: zibin@phas.ubc.ca

- [1] F. Finelli, J. Garcia-Bellido, A. Kovacs, F. Paci, and I. Szapudi (2014), arXiv:[1405.1555](#) [astro-ph.CO].
- [2] G. C. Omer, Proc. Nat. Acad. Sci. **53**, 1 (1965).
- [3] J. P. Zibin and A. Moss (2014), in preparation.
- [4] P. Ade et al. (Planck Collaboration) (2013), arXiv:[1303.5076](#) [astro-ph.CO].
- [5] I. Szapudi, A. Kovcs, B. R. Granett, Z. Frei, J. Silk, et al. (2014), arXiv:[1406.3622](#) [astro-ph.CO].
- [6] K. T. Inoue and J. Silk, Astrophys. J. **648**, 23 (2006), arXiv:[astro-ph/0602478](#) [astro-ph].
- [7] I. Masina and A. Notari, JCAP **0902**, 019 (2009), arXiv:[0808.1811](#) [astro-ph].
- [8] J. P. Zibin, Phys. Rev. **D78**, 043504 (2008), arXiv:[0804.1787](#) [astro-ph].
- [9] J. P. Zibin and A. Moss, Class. Quant. Grav. **28**, 164005 (2011), arXiv:[1105.0909](#) [astro-ph.CO].
- [10] J. P. Zibin, Phys. Rev. **D84**, 123508 (2011), arXiv:[1108.3068](#) [astro-ph.CO].
- [11] J. Zibin and D. Scott, Phys. Rev. **D78**, 123529 (2008), arXiv:[0808.2047](#) [astro-ph].
- [12] I. Szapudi, A. Kovcs, B. R. Granett, Z. Frei, J. Silk, et al. (2014), arXiv:[1405.1566](#) [astro-ph.CO].
- [13] N. Sakai and K. T. Inoue, Phys. Rev. **D78**, 063510 (2008), arXiv:[0805.3446](#) [astro-ph].
- [14] K. T. Inoue, N. Sakai, and K. Tomita, Astrophys. J. **724**, 12 (2010), arXiv:[1005.4250](#) [astro-ph.CO].
- [15] K. T. Inoue, Mon. Not. Roy. Astron. Soc. **421**, 2731 (2012), arXiv:[1109.4527](#) [astro-ph.CO].